catalysts

MDPI

Article

Ab Initio Studies of Bimetallic-Doped {0001} Hematite Surface for Enhanced Photoelectrochemical Water Splitting

Joseph Simfukwe [1,2,*], Refilwe Edwin Mapasha [1], Artur Braun [3] and Mmantsae Diale [1,*]

[1] Physics Department, University of Pretoria, Pretoria 0002, South Africa; edwin.mapasha@up.ac.za
[2] Physics Department, Copperbelt University, Riverside, Kitwe 10101, Zambia
[3] Laboratory for High Performance Ceramics, Empa, Swiss Federal Laboratories for Materials Science and Technology, CH-8600 Dübendorf, Switzerland; Artur.Braun@empa.ch
* Correspondence: joseph.simfukwe@cbu.ac.zm (J.S.); mmantsae.diale@up.ac.za (M.D.)

Abstract: First-principles calculations based on density functional theory (DFT) were carried out to study the energetic stability and electronic properties of a bimetallic-doped α-Fe_2O_3 photoanode surface with (Zn, Ti) and (Zn, Zr) pairs for enhanced PEC water splitting. The doped systems showed negative formation energies under both O-rich and Fe-rich conditions which make them thermodynamically stable and possible to be synthesised. It is found that in a bimetallic (Zn, Ti)-doped system, at a doping concentration of 4.20% of Ti, the bandgap decreases from 2.1 eV to 1.80 eV without the formation of impurity states in the bandgap. This is favourable for increased photon absorption and efficient movement of charges from the valance band maximum (VBM) to the conduction band minimum (CBM). In addition, the CBM becomes wavy and delocalised, suggesting a decrease in the charge carrier mass, enabling electron–holes to successfully diffuse to the surface, where they are needed for water oxidation. Interestingly, with single doping of Zr at the third layer (L3) of Fe atoms of the {0001} α-Fe_2O_3 surface, impurity levels do not appear in the bandgap, at both concentrations of 2.10% and 4.20%. Furthermore, at 2.10% doping concentration of α-Fe_2O_3 with Zr, CBM becomes delocalised, suggesting improved carrier mobility, while the bandgap is altered from 2.1 eV to 1.73 eV, allowing more light absorption in the visible region. Moreover, the photocatalytic activities of Zr-doped hematite could be improved further by codoping it with Zn because Zr is capable of increasing the conductivity of hematite by the substitution of Fe^{3+} with Zr^{4+}, while Zn can foster the surface reaction and reduce quick recombination of the electron–hole pairs.

Keywords: first principles; bimetallic doping; water splitting; bandgap

Citation: Simfukwe, J.; Mapasha, R.E.; Braun, A.; Diale, M. Ab Initio Studies of Bimetallic-Doped {0001} Hematite Surface for Enhanced Photoelectrochemical Water Splitting. *Catalysts* **2021**, *11*, 940. https://doi.org/10.3390/catal11080940

Academic Editor: Tzu-Hsuan Chiang

Received: 23 June 2021
Accepted: 19 July 2021
Published: 3 August 2021

1. Introduction

Photoelectrochemical water splitting (PEC-WS), using sunlight and appropriate semiconductors (SCs) to split water molecules into constituent hydrogen (H_2) and oxygen (O_2) gases, is a promising route to solve both the production of clean H_2 fuel and storage for solar energy. Since the demonstration of the first PEC cell by Fujishima and Honda in 1972 [1], significant research efforts have been directed toward the development of new photoelectrode materials that can efficiently harvest solar energy and catalyse the photoelectrolysis of water into molecular O_2 and H_2 [2]. A large number of inorganic materials have been studied as photoelectrodes for PEC-WS [3]. Of interest have been particularly semiconductors such as TiO_2 [1,4,5], WO_3 [4–6], $BiVO_4$ [4,5,7], and α-Fe_2O_3 (hematite) [4,5,8,9] as photoanode materials for PEC devices. Compared to other semiconductors, hematite stands out [10] as photoanode material due to its various advantages such as a favourable bandgap, ranging from 1.9 to 2.2 eV [2,4,11–15], capable of absorbing about 40% solar energy with a potential of converting 16.8% of this energy into H_2 fuel [4,8,15,16], high stability in aqueous solutions, nontoxicity, abundant and cost effective. On the other hand, its poor electrical conductivity [17–19], low carrier mobility (<1 $cm^2\ V^{-1}\ s^{-1}$) [2,4,16], short hole diffusion length (~2 to 4 nm) [2,4,16,20], and fast recombination of the charge carriers

(~10 ps) [4,18–20] have limited its full potential for PEC applications. Moreover, the CBM of α-Fe_2O_3 lies ~0.2 eV below the H^+/H_2 redox potential [14,21–23]. Therefore, an electrical voltage is needed for H_2 evolution at the cathode.

To overcome these challenges, different approaches such as nanostructuring, heterojunctions, incorporating conducting scaffolds, surface modification, and doping have been explored both theoretically and experimentally [13,14]. Doping is well known to increase the carrier concentration leading to improved electron conductivity, extended lifetime of photo-generated charge carriers [24], decreased bandgap, and increased absorption spectrum of the SC [25,26]. Despite several positive reports on doping [9,18,19,25,27–29], negative effects of bulk doped systems, for example, induced impurity states in the band structure which act as recombination centres for electron–hole pairs have been reported [2,19,30,31]. One way of circumventing the problem of charge recombination in hematite is surface doping at or near the surface (surface doping). Surface doping can strengthen the PEC performance of α-Fe_2O_3 by fostering interfacial charge transfer to adsorbates [13,32,33].

In addressing the performance enhancement of photoelectrodes, it is important to realise that a photoelectrode has at least a twofold task. First, it absorbs photons and converts them into electric charge carriers; this is accomplished usually by the bulk of the electrode material because light absorption and conversion occur over the absorption length and thus via the volume of the electrode [34]. An entirely different task is the use of the charge carriers in the chemical splitting of water into H_2 and O_2. This chemical reaction occurs at the surface and may require a different electronic and molecular structure of the material than underneath in the bulk.

In our immediate past study [13], the effect of Zn on the {0001} and $\{01\bar{1}2\}$ surfaces was studied. The study showed that when doped on layer L1 of the {0001} surface, Zn can both narrow the bandgap and eliminate unwanted states in the band structure. However, when doping was performed slightly deep on layers L2 and L3 of the {0001} surface, localised states appeared above VBM which may trap the created electron–hole pairs. With an understanding that Zn has the potential of enhancing the separation of electrons and holes at the surface, thereby reducing the quick recombination of the charge carriers [5,35,36], our focus in this study is to explore strategies that can circumvent the challenge of localised impurity states which appeared in layers L2 and L3 of our previous study upon monodoping with Zn [13]. This can be carried out by codoping anion with cation which is an effective way of increasing the solubility of the dopants in the crystal lattice and strengthening the conductivity of the SC material [5,19,30,37–39].

In this study, first-principles calculations based on density functional theory were carried out to study the energetic stability and electronic properties of bimetallic-doped {0001} α-Fe_2O_3 surface with (Zn, Ti) and (Zn, Zr) pairs for enhanced PEC water splitting. Bimetallic doping is an important and executable way of increasing the conductivity of semiconductor materials and reducing the quick recombination of the electron–hole pairs [5,40–42]. Recently, Mirbagheri et al. [4], and later, Zhu et al. [5] carried out a (Zn, Ti) codoping on bulk hematite and found that Zn dopant was capable of reducing the recombination of the charge carriers, while Ti increased the conductivity and carrier density of α-Fe_2O_3. This resulted in a 2.5-times enhancement of the photocurrent density than that of undoped hematite. Kaouk et al. [40] codoped hematite with (In, Sn) and reported an increase in PEC efficiency which they attributed to higher electron mobility and reduced recombination of the electron–hole pairs. Wang et al. [41] synthesised (Co, Sn)-codoped α-Fe_2O_3 and found that Sn doping increased carrier density of α-Fe_2O_3, while Co improved the surface reactions. Our results showed negative formation energies for all doped systems under both O-rich and Fe-rich conditions which make them thermodynamically stable and possible to be synthesised in the laboratory. It is found that in a bimetallic (Zn, Ti) doped system, at a doping concentration of 4.20% of Ti, the bandgap decreases from 2.1 eV to 1.80 eV with no impurity state in the band structure which is favourable for increased photon absorption and efficient movement of charges from VBM to CBM. Interestingly, we

find that with single doping of Zr at the third layer (L3) of Fe atoms of the {0001} α-Fe_2O_3 surface, impurity levels do not appear in the band structure, at both concentrations of 2.10% and 4.20%.

2. Results and Discussions

2.1. Energetic Stability of the Doped Systems

One important parameter to evaluate thermodynamic stability and optimal growth conditions in experiments for doped systems is formation energy (E_{form}). E_{form} provides important information in understanding the relative difficulty of incorporating the dopant elements into the host lattice in experiments [30,43]. Therefore, E_{form} for all the doped systems had to be evaluated using Equations (1) and (2).

$$E(X\ doped)_{form} = E(X\ doped) - E(pure) - n\mu_X + n\mu_{Fe} \quad (1)$$

$$E(X, Zn\ \ doped)_{form} = E(X, Zn\ \ doped) - E(pure) - n_{zn}\mu_{Zn} - n_X\mu_X + m\mu_{Fe} \quad (2)$$

where $E(pure)$, $E(X\ doped)$ and $E(X, Zn\ \ doped)$ are the total energies of the pristine surface, mono, and bimetallic-doped systems, respectively, where (X = Ti or Zr). μ_X,μ_{Zn}, and μ_{Fe} are the chemical potentials of X, Zn, and Fe, respectively; n is the number of X atoms in substitution of Fe atoms in a mono doped system; n_X and n_{Zn} is the number of X and Zn atoms substituting Fe atoms in the bimetallic doped system, respectively, where $m = n_X + n_{Zn}$. As stated earlier, E_{form} is strongly related to the growth conditions of the doped systems in experiments which could vary between O-rich and Fe-rich conditions (known as oxidising and reducing atmosphere for synthesis and processing of ceramic materials) [19,30]. To obtain the chemical potentials μ_{Fe} and μ_O, Equation (3) must be satisfied [19,30,33], where $\mu_{Fe_2O_3}$ is the total energy of the α-Fe_2O_3 unit cell.

$$2\mu_{Fe} + 3\mu_O = \mu_{Fe_2O_3} \quad (3)$$

For O-rich limits, μ_O is obtained from, while μ_{Fe} is calculated from the restrictive conditions in Equation (3). In an O-poor environment, μ_{Fe} corresponds to the energy of a single atom of Fe in its stable bulk α-Fe, while μ_O is calculated using Equation (3). Figure 1 depicts (a) mono X-doped, (b) bimetallic (Zn, X)-doped, and (c) bimetallic (Zn, 2X)-doped {0001) surfaces. The calculated formation energy E_{form} of all the doped {0001) hematite systems is presented in Table 1.

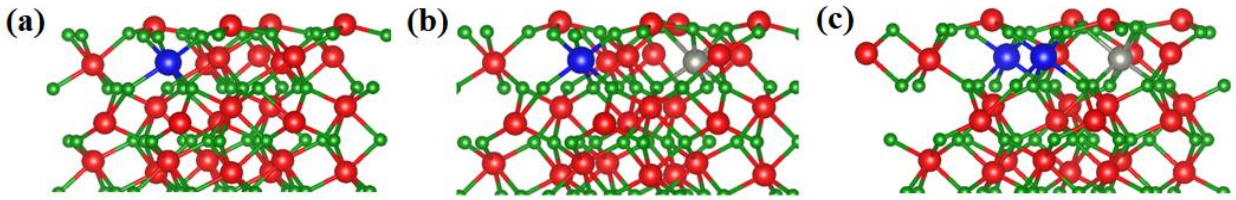

Figure 1. The relaxed mono and bimetallic doped {0001) surfaces: (**a**) mono X doped, (**b**) bimetallic (Zn, X) doped, and (**c**) bimetallic (Zn, 2X) doped. Colour scheme: red (big spheres) and green (small spheres) denote Fe and O atoms, respectively; blue and grey (big sphere) represent X and Zn atoms, where (X = Ti or Zn).

Table 1. E_{form} of mono and bimetallic-doped {0001} hematite systems in O-rich (oxidising) and Fe-rich (reducing) conditions.

Dopants	Formation Energy (eV)	
	Fe-Rich	O-Rich
Ti	−3.59	−5.10
(Zn, Ti)	1.46	−1.59
(Zn, 2Ti)	−0.39	−4.93
Zr	−2.25	−3.76
2Zr	−8.21	−11.23
(Zn, Zr)	−4.34	−7.37
(Zn, 2Zr)	−5.32	−9.87

From Table 1, we notice that the formation energy for one Ti or Zr atom substituting Fe atom in the {0001} α-Fe_2O_3 surface is negative in both O-rich and Fe-rich conditions, in agreement with Pan et al. [19]. This implies that Ti dopant can easily be incorporated in the {0001} surface and also that the structure is thermodynamically stable. As for the bimetallic (Zn, Ti)-doped system, E_{form} is negative in the O-rich condition, while it is positive in the Fe-rich condition. This indicates that bimetallic doping of (Zn, Ti) is favoured under oxidising conditions and not under reducing conditions. We thus can provide recommendations for synthetic chemists and processing engineers for the synthesis of the materials. Furthermore, we notice that when the concentration of Ti is increased in the bimetallic-doped system from (Zn, Ti) to (Zn, 2Ti), representing a change of concentration from 2.1% to 4.2% for Ti dopant, E_{form} becomes negative in both O-rich and Fe-rich. This shows an increase in the stability of the (Zn, Ti)-codoped system, with the increasing concentration of Ti atoms. The rest of the doped structures Zr, 2Zr, (Zn, Zr), and (Zn, 2Zr) show that their incorporation in the host lattice is relatively easy to achieve under both O-rich and Fe-rich and could be synthesised, as inferred by their negative formation energies.

2.2. Charge Density Difference Plots

In a quest to understand the nature of bonding and charge distribution among the atoms of the mono and bimetallic-doped {0001} hematite system, the charge density difference ($\Delta\rho$) [33,44–46] is plotted using Equation (4).

$$\Delta\rho = \rho^{total} - \sum_i \rho_i^{fragments} \quad (4)$$

where ρ^{total} and $\rho_i^{fragments}$ are the total and individual fragments charge density of the system, respectively. $\rho_i^{fragments}$ is calculated from a pseudo structure in which the i-th fragment is kept in place, while the other fragments are deleted. The lattice parameters and symmetry of the pseudo structure remain the same as the original supercell. Figure 2 presents the top and side views of the $\Delta\rho$ plots for (a) mono-doped *X* element (b) bimetallic-doped (Zn, *X*), and (c) bimetallic-doped (Zn, 2*X*) of {0001} α-Fe_2O_3 at the isosurface value of 0.020 electrons/bohr^3. It is seen that in all the three doped systems (a, b, and c), the concentration of charges is at the top of the surface, similar to our earlier observations in the previous studies [13,33]. It is further observed that more charges depleted (denoted by cyan colour) from the dopant elements (Ti, Zr, and Zn) and accumulated (denoted by the yellow colour) on the surrounding Fe and O atoms. The Bader charger analysis [47] revealed that on average Ti, Zr and Zn donated 2.20 e, 2.53 e, and 1.37 e, respectively, to form bonds with adjacent O atoms. It is proved that surface doping is advantageous because the charge carriers are formed in the vicinity of reaction centres with hydroxyl adsorbate, overcoming the issue of short diffusion lengths in α-Fe_2O_3 [32,33].

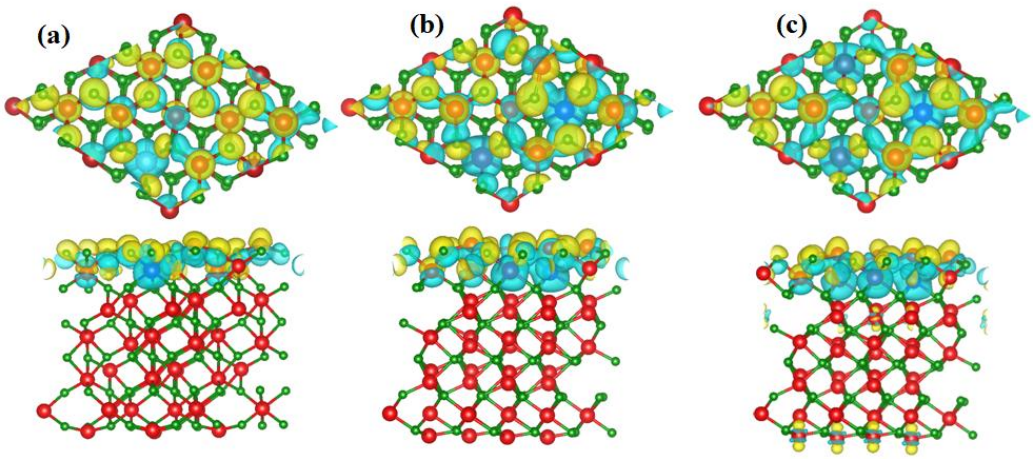

Figure 2. Charge density difference plots top and side views of (**a**) mono-doped *X* element (**b**) bimetallic-doped (Zn, *X*), and (**c**) bimetallic-doped (Zn, 2*X*) of {0001} surface; yellow and cyan colours show accumulation and depletion of charge density, respectively.

2.3. Electronic Band Structure and Density of States

Figure 3 presents the PDOS and band structure of pristine {0001} surface (a,b) Ti doped (c,d) and (Zn, Ti) codoped (e,f). In Figure 3a, it is noted that the VBM of the pristine surface comprises mainly of O 2p states with a small portion of Fe 3 d states, while the CBM is composed of largely the Fe 3 d orbitals. The calculated bandgap of the pristine surface is 2.10 eV [13,33]. Moreover, when one Fe atom is replaced by one Ti atom, as depicted in Figure 1a, corresponding to a doping concentration of 2.10%, an impurity state comprising of Ti 3d states and O 2p states appears within the band structure, as seen in Figure 3c,d, similar to what was found in another study [19]. The calculated bandgap of Ti-doped {0001} hematite surface is 1.93 eV which shows a decrease from the pristine surface bandgap of 2.10 eV. The decrease in the bandgap implies more photon absorption in the visible spectrum leading to improved PEC performance. However, the impurity state in the band structure may reduce the carrier mobility and also act as a recombination centre for the electron–hole pairs, resulting in low PEC performance [19,30].

Moreover, Zhu et al. [5] argue that among the dopants that have been incorporated in hematite, Ti stands out because of its ability to increase the photocurrent significantly through enhanced conductivity and carrier density. However, Ti's capability to resolve the challenge of recombination of electron–hole pairs is comparatively limited. The solution to this challenge lies in codoping Ti with a p-type element such as Zn [4,5,30]. Many studies have shown that Zn is a p-type dopant for α-Fe_2O_3, while Ti is an n-type element [5,19,28,36,48,49]. Therefore, the combination of (Zn, Ti) forms an acceptor–donor pair. Codoping both n-type and p-type elements is expected to offset the negative effects aroused by each element while at the same time enhancing their positive effects. Additionally, Zn is capable of promoting faster charge transfer at the surface, resulting in reduced recombination of the electron–hole pairs [4,5]. Therefore, the combination of Zn with Ti or Zr is expected to improve the PEC performance of hematite due to increased conductivity and improved surface reaction kinetics. As stated earlier, Figure 3e,f presents PDOS and band structure of (Zn, Ti) codoped {0001} hematite surface. It is inferred from Figure 3e,f that although the codoping localised acceptor states consisting of Zn 3d orbitals and O 2p orbitals appear above the VBM of the surface, the Fermi level embeds in the VBM due to the upshift in the valence band edge, and the bandgap narrows down to 1.70 eV. We observe that although there is an appreciable decrease in the bandgap and an upshift in the CBM, compared to mono-doped Ti which effectively suggests increased photocatalytic efficiency of the {0001} hematite surface, the PEC activity is not likely to increase much due to localised acceptor states.

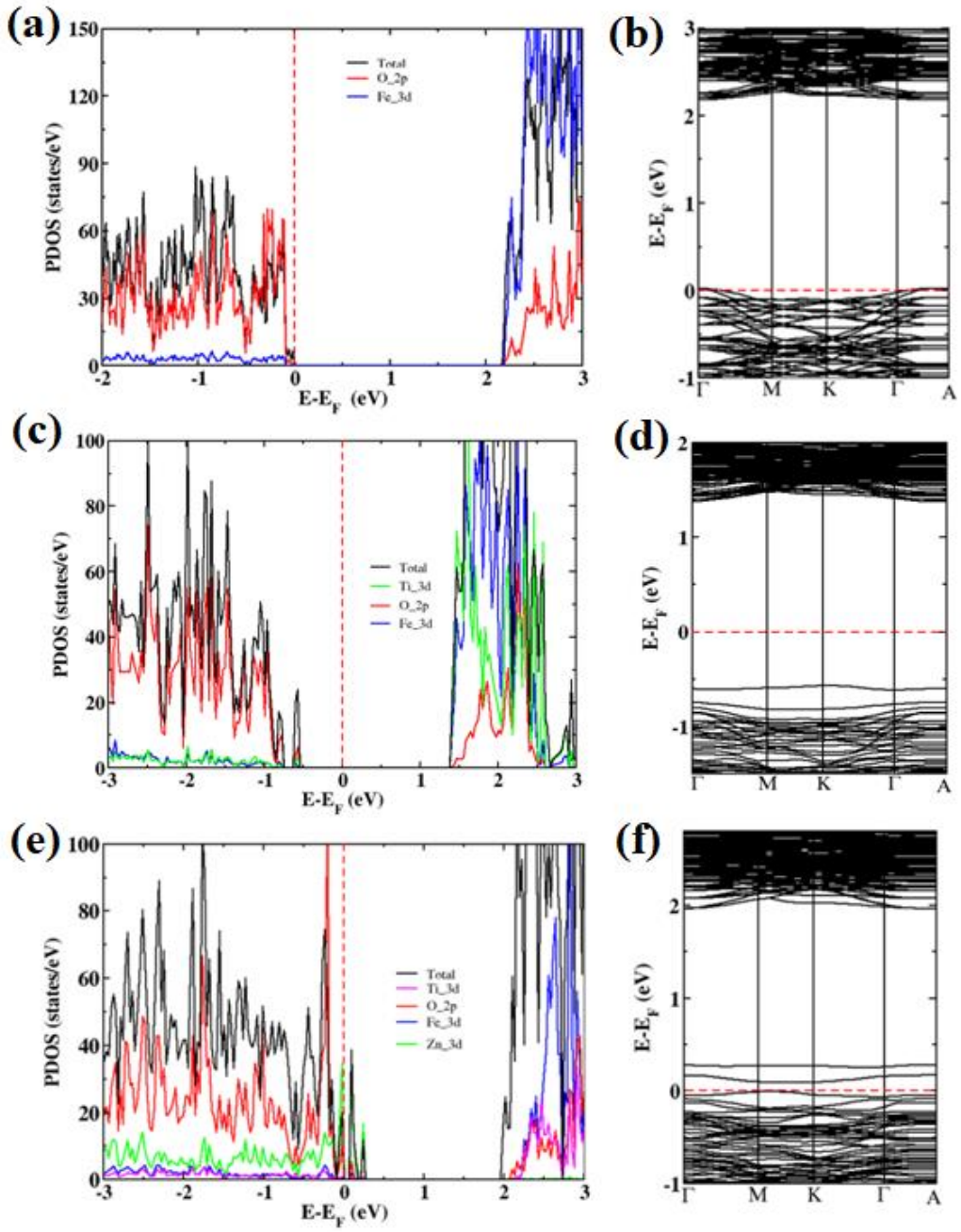

Figure 3. PDOS and band structure of pristine {0001} α-Fe_2O_3 surface (**a**,**b**), (Ti)-doped {0001} α-Fe_2O_3 surface (**c**,**d**), and (Zn, Ti)-doped {0001} α-Fe_2O_3 surface (**e**,**f**). The Fermi level is set to zero.

On the other hand, we notice from Figure 4a,b that when the concentration of Ti is increased in the bimetallic-doped {0001} surface from 2.10% (Zn, Ti) to 4.20% (Zn, 2Ti), the localised states within the band structure are eliminated, while the bandgap decreases to 1.80 eV. Zhu et al. [5] carried out both an experimental and a theoretical study of (Ti, Zn)-codoped bulk hematite and reported an increased photocurrent density when the concentration of Ti was raised from 1% to 3%. They further pointed out that the detrimental effect of Zn dopant may overweigh its positive effect when the concentration of Ti dopant is low. Thus, there must be a good quantity control of dopant concentration to coordinate well the delicate balance between the two dopants in attaining a higher PEC performance of hematite. We note that the absence of impurity states in the band structure due to increased concentration of Ti dopant which also increases the charge carrier density, coupled with the decrease in the bandgap, is likely to increase the PEC performance in a bimetallic (Zn,

2Ti)-doped α-Fe_2O_3. Additionally, the CBM in Figure 4b becomes wavy and delocalised, suggesting a decrease in the charge carrier mass, enabling them to successfully diffuse to the surface where they are needed for hydrogen evolution [13,19].

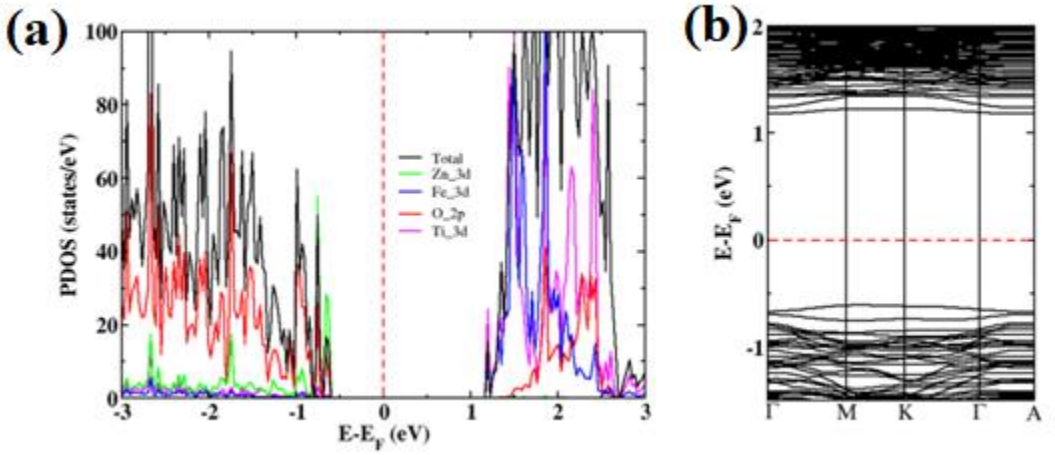

Figure 4. PDOS (**a**) and band structure of (Zn, 2Ti)-codoped {0001} α-Fe_2O_3 surface (**a**,**b**). The Fermi level is set to zero.

Since Ti and Zr have similar outer electronic structures, we further examined the effects of Zr and Zr codoped with Zn (Zn, Zr) on the {0001} α-Fe_2O_3 surface. The calculated PDOS and band structure for Zr-doped {0001} α-Fe_2O_3 surface systems are shown in Figure 5. With 2.10% of Fe atoms replaced by Zr atoms, CBM moves towards VBM, and the bandgap decreases to 1.73 eV from the initial 2.1 eV. Moreover, the CBM in Figure 5b becomes delocalised, suggesting improved carrier mobility, as earlier noted. VBM mainly constitutes of O 2p states and the 4d states of Zr, while CBM is composed of O 2p states, Fe 3d states, and Zr 4d states.

When the concentration of Zr was raised from 2.10% (Zr) to 4.20% (2Zr), CBM moved further towards VBM. However, the bandgap remained unchanged, compared to the pristine surface at 2.10 eV because VBM also moved towards the lower energy. Interestingly, we observe that with single doping of Zr at the third layer (L3) of Fe atoms, as depicted in Figure 1a of the {0001} α-Fe_2O_3 surface, impurity levels do not appear in the band structure, at both concentrations of 2.10% and 4.20%. Experimentally, Kumar et al. [50] doped α-Fe_2O_3 nanostructured with Zr at various concentrations and recorded the highest photocurrent density of 2.1 mA/cm^2 at a doping concentration of 2.0 at.% Zr.

The calculated bandgap energy for all their doped hematite samples was ~2.10 eV. They inferred that since there was no change in the bandgap energy of all the Zr-doped α-Fe_2O_3 samples, Zr doping may not produce any intermediate level within the band structure of α-Fe_2O_3. Using DFT calculations, our results show that at the doping concentration of 2.10% of Zr atoms, the bandgap can be narrowed to 1.73 eV, and no unwanted states are present, while at 4.20% doping concentration, the bandgap remains unchanged, in agreement with Kumar et al. [50]. Moreover, apart from the substitutional doping of Fe^{3+} by Zr^{4+} in α-Fe_2O_3 lattice as the source of the enhanced photocurrent density, the decrease in the bandgap of 1.73 eV at 2.10% doping concentration and the removal of unwanted states in the band structure and the delocalisation of CBM are other microscopic sources for improved PEC activity of Zr doped hematite.

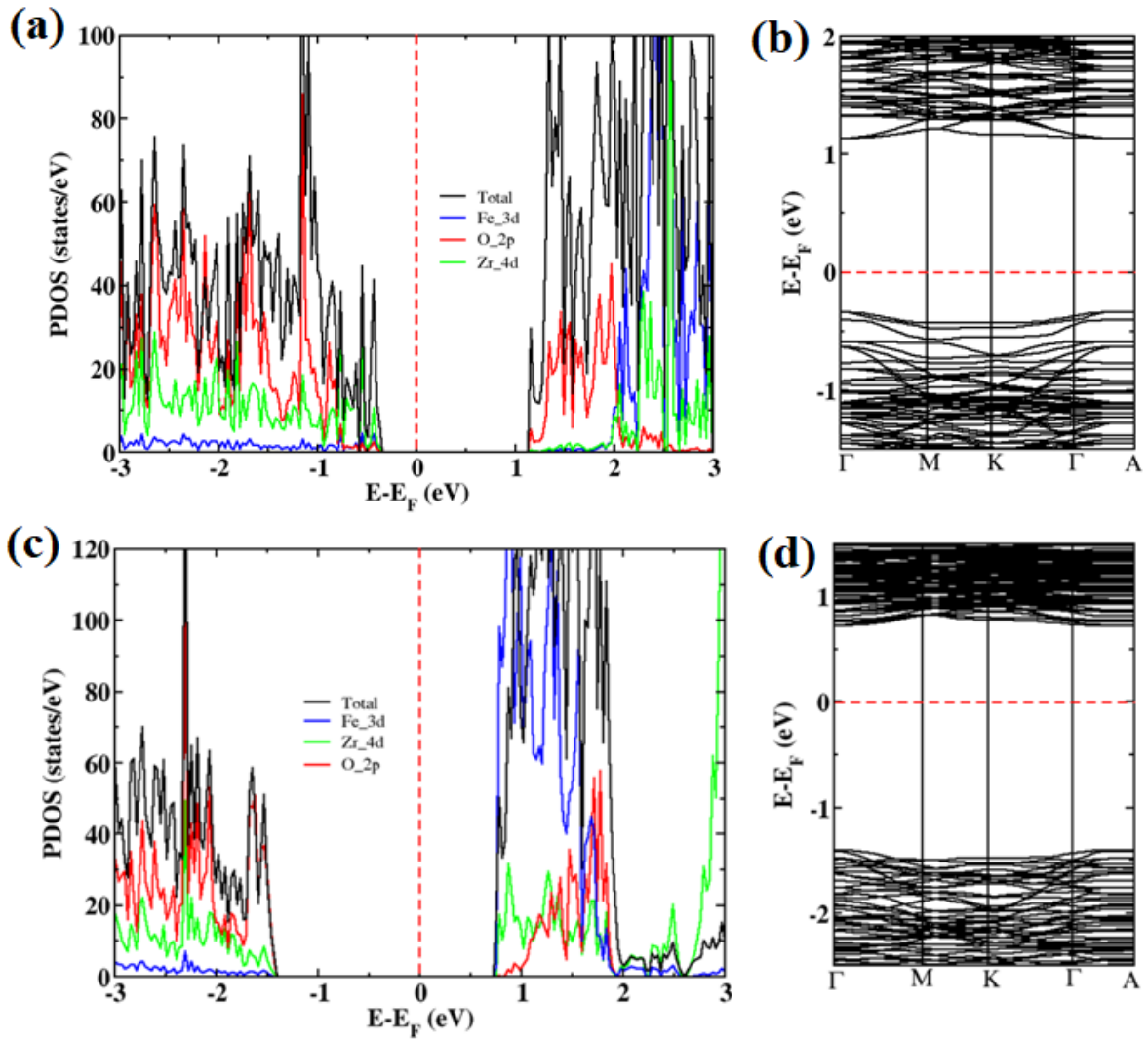

Figure 5. PDOS and band structure of Zr-doped {0001} α-Fe_2O_3 surface (**a**,**b**) and (2Zr)-doped {0001} α-Fe_2O_3 surface (**c**,**d**). The Fermi level is set to zero.

The photocatalytic activities of Zr-doped hematite could be improved further by codoping it with Zn for the reasons advanced earlier. Zr, being an n-type dopant [19,50], has the potential of increasing the conductivity and carrier density of α-Fe_2O_3, while Zn, as a p-type dopant, could foster the surface reaction and reduce recombination of the electron–hole pairs [5,51]. In Figure 6, the calculated PDOS and band structure for Zr-codoped with Zn at 2.10% (Zn, Zr) and 4.20% Zr concentration (Zn, 2Zr) are presented. It is found that in both systems, no impurity states appeared in the band structure which is favourable for the mobility of the charge carriers from VBM to CBM. VBM at 2.10% and 4.20% Zr concentrations consists of O 2p orbitals, Zn 3d orbitals, and Zr 4d orbitals, while CBM constitutes mainly of Fe 3d and Zr 4d orbitals, with a small portion of O 2p orbitals. It is also observed that the concentration of Zr 4d states is more in CBM of the 4.20%-doped system which may be the reason for the upward shift of CBM, as compared to the other two Zr mono-doped systems in Figure 5 and the 2.10% (Zn, Zr- codoped system, presented in Figure 6a,b. The bandgaps for both systems remain almost unchanged, as compared to the pristine surface at 2.09 eV and 2.08 eV, respectively.

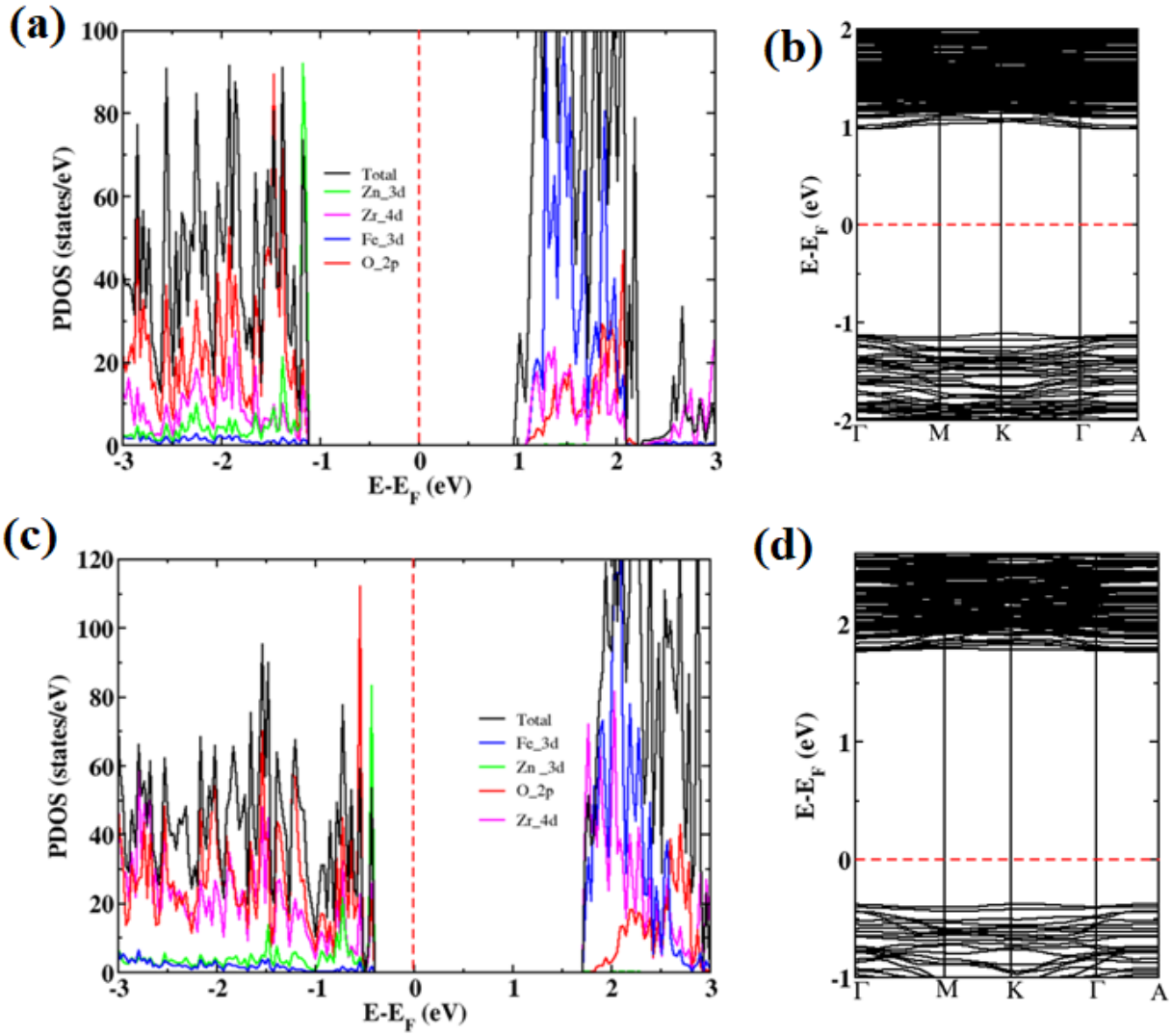

Figure 6. PDOS and band structure of (Zn, Zr)-codoped {0001} α-Fe_2O_3 surface (**a**,**b**) and (Zn, 2Zr)-codoped {0001} α-Fe_2O_3 surface (**c**,**d**). The Fermi level is set to zero.

To examine how these dopants influenced the band edge positions, we plotted the VBM and CBM of the doped systems and compared them with pristine hematite, as shown in Figure 7. It is observed that apart from (Zn, Ti)-doped pair at 2.10% concentration whose CBM and VBM were raised by 0.10 eV and 0.11 eV, respectively, with respect to pristine α-Fe_2O_3, the rest of the doped system had their CBM and VBM lowered. This implies that in addition to the positive effects brought about by these dopants on α-Fe_2O_3 which we have discussed earlier, a bias voltage will still be needed to elevate CBM for the production of H_2. It is also interesting to note that (Zn, 2Zr) codoped at 4.20% Zr concentration had its CBM lowered by 0.14 eV, compared to that of pristine α-Fe_2O_3 which means a lower bias voltage may be required for this system, as compared to others.

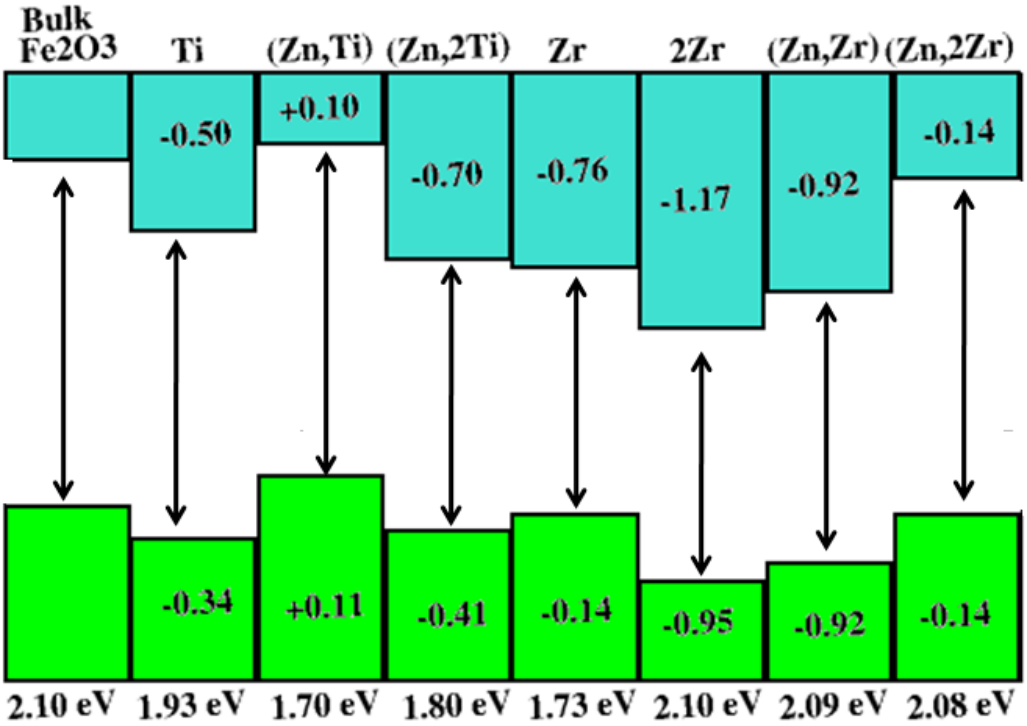

Figure 7. VBM and CBM positions of doped systems as calculated with respect to that of bulk α-Fe_2O_3. The plus (+) and minus (−) signs denote up or downshifting of the bands with reference to VBM and CBM of bulk α-Fe_2O_3, respectively.

3. Method

All calculations were performed using the DFT method [52,53], as implemented within the plane–wave (PW) quantum–espresso code [54]. The Vanderbilt Ultrasoft Pseudopotential (USPPs) [55] were used to describe the valence electrons, while the exchange and correlation energies are treated at the level GGA of PBE [56]. Generally, the standard DFT exchange–correlation functionals such as the local density approximation (LDA) and the GGA fail to correctly describe systems characterised by strongly correlated and typically localised *d* or *f* electrons [57–60]. This failure is mainly due to the incomplete cancellation of the Hartree self-interaction error resulting in over-delocalisation of the *f* and *d* electrons [59] and also the absence of integer discontinuity in the exchange and correlation energy. One of the simplest approaches to correct this error is to use DFT with on-site coulomb energy (DFT+U), based on the corrective functional inspired by the Hubbard model [61,62]. Consequently, we used the DFT+U method with the converged U = 5 eV [13,33,63–65] to correctly study the electronic structure of bulk and doped surfaces of hematite (α-Fe_2O_3). A kinetic energy cut-off of 350 eV was used in the expansion of the electronic wave function in the PW basis set. The energy convergence threshold was set to 10^{-5} eV and 10^{-2} eV/Å for the force. A vacuum space of 20 Å was introduced to avoid interactions between the periodic surface images. A supercell method was used to examine the influence of Zn, Ti, and Zr on the energetic stability and electronic properties of the {0001} surface. The Brillouin zone integration was performed with Monkhorst-Pack (MP) k-point grids [66] of $2 \times 2 \times 1$ and $6 \times 6 \times 2$ for the calculations of the total energies and the density of states (DOS), respectively, for the 120 atoms in a supercell surface.

4. Conclusions

We examined the energetic stability and electronic properties of bimetallic-doped {0001} α-Fe_2O_3 surface for enhanced PEC water splitting using DFT calculations. The doped systems showed negative formation energies under both O-rich and Fe-rich conditions which make them thermodynamically stable and possible to be prepared experimentally.

The results show that bimetallic doping decreases the bandgap without impurity state in the band structure which is favourable for increased photon absorption and efficient movement of charges from VBM to CBM. In addition, CBM becomes wavy and delocalised, suggesting a decrease in the charge carrier mass enabling them to successfully diffuse to the surface where they are needed for hydrogen evolution. Moreover, single doping of Zr at layer 3 (L3) of Fe atoms of {0001} α-Fe_2O_3 surface, impurity levels can be eliminated in the band structure. Furthermore, the PEC activities of Zr-doped hematite could be improved further by codoping it with Zn because Zr is capable of increasing the conductivity of hematite by the substitution of Fe^{3+} with Zr^{4+}, while Zn can foster the surface reaction and reduce quick recombination of the electron–hole pairs. It is proved that surface doping is advantageous because the charge carriers are formed in the vicinity of reaction centres with the adsorbates, overcoming the challenge of short diffusion length in α-Fe_2O_3. Bimetallic doping of (Zn, Ti) and (Zn, Zr) on the {0001} surface is expected to enhance the PEC performance of hematite due to the advantages of both surface and bimetallic doping. According to our knowledge, the study on Zn being codoped with Zr is being carried out for the first time, and therefore, we hope that our results provided here will be of great interest to both experimentalist and theoretical researchers.

Author Contributions: Conceptualization, J.S., A.B. and M.D.; methodology, J.S. and R.E.M.; software J.S., R.E.M. and M.D.; validation, All authors; formal analysis All authors; Investigation, J.S. and R.E.M.; Resources, M.D.; data curation, J.S. and A.B.; writing-original draft preparation, J.S.; writing-review and editing, All authors; visualisation, All authors; supervision, M.D.; funding acquisition, J.S., A.B. and M.D.; payment of APC, M.D. All authors have read and agreed to the published version of the manuscript.

Funding: This research was funded by the Copperbelt University and Ministry of Higher Education in Zambia through the Support to Science Technology and Engineering Project (SSTEP), SSTEP_2016-2020; it also was fund by 149031 Production of Liquid Solar Fuels from CO2 and Water: Using Renewable Energy Resources Swiss South African Joint Research Programme (SSAJRP) NRF—Research Foundation, IZLSZ2_149031.

Acknowledgments: This work emerged from the Swiss South-Africa Joint Research Programme project "IZLSZ2_149031 Production of Liquid Solar Fuels from CO2 and Water: Using Renewable Energy Resources Swiss South African Joint Research Programme (SSAJRP) NRF—National Research Foundation". The Copperbelt University and Ministry of Higher Education in Zambia through the Support to Science, Technology and Engineering Project (SSTEP). The University of Pretoria and the Centre for High-Performance Computing (CHPC) Cape Town, South Africa are strongly acknowledged for their cluster resources.

Conflicts of Interest: The authors declare no conflict of interest.

References

1. Fujishima, A.; Honda, K. Electrochemical Photolysis of Water at a Semiconductor Electrode. *Nat. Cell Biol.* **1972**, *238*, 37–38. [CrossRef] [PubMed]
2. Barroso, M.; Pendlebury, S.R.; Cowan, A.J.; Durrant, J.R. Charge Carrier Trapping, Recombination and Transfer in Hematite (A-Fe_2O_3) Water Splitting Photoanodes. *Chem. Sci.* **2013**, *4*, 2724–2734. [CrossRef]
3. Ahmed, S.M.; Leduc, J.; Haller, S.F. Photoelectrochemical and impedance characteristics of specular hematite. 1. Photoelectrochemical parallel conductance, and trap rate studies. *J. Phys. Chem.* **1988**, *92*, 6655–6660. [CrossRef]
4. Mirbagheri, N.; Wang, D.; Peng, C.; Wang, J.; Huang, Q.; Fan, C.; Ferapontova, E.E. Visible Light Driven Photoelectrochemical Water Oxidation by Zn-and Ti-Doped Hematite Nanostructures. *Acs Catal.* **2014**, *4*, 2006–2015. [CrossRef]
5. Zhu, Q.; Yu, C.; Zhang, X. Ti, Zn co-doped hematite photoanode for solar driven photoelectrochemical water oxidation. *J. Energy Chem.* **2019**, *35*, 30–36. [CrossRef]
6. Su, J.; Feng, X.; Sloppy, J.D.; Guo, L.; Grimes, C.A. Vertically Aligned WO3 Nanowire Arrays Grown Directly on Transparent Conducting Oxide Coated Glass: Synthesis and Photoelectrochemical Properties. *Nano Lett.* **2011**, *11*, 203–208. [CrossRef]
7. Jia, Q.; Iwashina, K.; Kudo, A. Facile fabrication of an efficient BiVO4 thin film electrode for water splitting under visible light irradiation. *Proc. Natl. Acad. Sci. USA* **2012**, *109*, 11564–11569. [CrossRef]
8. Sivula, K.; Le Formal, F.; Grätzel, M. Solar Water Splitting: Progress Using Hematite (α-Fe_2O_3) Photoelectrodes. *ChemSusChem* **2011**, *4*, 432–449. [CrossRef]

9. Ling, Y.; Wang, G.; Wheeler, D.A.; Zhang, J.Z.; Li, Y. Sn-Doped Hematite Nanostructures for Photoelectrochemical Water Splitting. *Nano Lett.* **2011**, *11*, 2119–2125. [CrossRef]
10. Bora, D.K.; Braun, A.; Constable, E.C. "In Rust We Trust". Hematite–the Prospective Inorganic Backbone for Artificial Photosynthesis. *Energy Environ. Sci.* **2013**, *6*, 407–425. [CrossRef]
11. Liao, P.; Keith, J.A.; Carter, E.A. Water Oxidation on Pure and Doped Hematite (0001) Surfaces: Prediction of Co and Ni as Effective Dopants for Electrocatalysis. *J. Am. Chem. Soc.* **2012**, *134*, 13296–13309. [CrossRef] [PubMed]
12. Podsiadły-Paszkowska, A.; Tranca, I.C.; Szyja, B.M. Tuning the Hematite (110) Surface Properties to Enhance Its Efficiency in Photoelectrochemistry. *J. Phys. Chem. C* **2019**, *123*, 5401–5410. [CrossRef]
13. Simfukwe, J.; Mapasha, R.E.; Braun, A.; Diale, M. Exploring the Stability and Electronic Properties of Zn-Doped Hematite Surfaces for Photoelectrochemical Water Splitting. *J. Phys. Chem. Solids* **2019**, *136*, 109159. [CrossRef]
14. Tamirat, A.G.; Rick, J.; Dubale, A.A.; Su, W.-N.; Hwang, B.-J. Using Hematite for Photoelectrochemical Water Splitting: A Re-view of Current Progress and Challenges. *Nanoscale Horiz.* **2016**, *1*, 243–267. [CrossRef]
15. Le Formal, F.; Grätzel, M.; Sivula, K. Controlling Photoactivity in Ultrathin Hematite Films for Solar Water-Splitting. *Adv. Funct. Mater.* **2010**, *20*, 1099–1107. [CrossRef]
16. Franking, R.; Li, L.; Lukowski, M.A.; Meng, F.; Tan, Y.; Hamers, R.J.; Jin, S. Facile Post-Growth Doping of Nanostructured Hem-atite Photoanodes for Enhanced Photoelectrochemical Water Oxidation. *Energy Environ. Sci.* **2013**, *6*, 500–512. [CrossRef]
17. Gan, J.; Lu, X.; Tong, Y. Towards highly efficient photoanodes: Boosting sunlight-driven semiconductor nanomaterials for water oxidation. *Nanoscale* **2014**, *6*, 7142–7164. [CrossRef] [PubMed]
18. Pan, H.; Cai, J.; Meng, X.; Li, S.; Qin, G. 4d transition-metal doped hematite for enhancing photoelectrochemical activity: Theoretical prediction and experimental confirmation. *RSC Adv.* **2015**, *5*, 19353–19361. [CrossRef]
19. Pan, H.; Qin, G.; Meng, X.; Liu, N.; Li, S. (Ti/Zr,N) codoped hematite for enhancing the photoelectrochemical activity of water splitting. *Phys. Chem. Chem. Phys.* **2015**, *17*, 22179–22186. [CrossRef] [PubMed]
20. Pan, H.; Meng, X.; Qin, G. Hydrogen Generation by Water Splitting on Hematite (0001) Surfaces: First-Principles Calculations. *Phys. Chem. Chem. Phys.* **2014**, *16*, 25442–25448. [CrossRef]
21. Glasscock, J.A.; Barnes, P.; Plumb, I.C.; Savvides, N. Enhancement of Photoelectrochemical Hydrogen Production from Hematite Thin Films by the Introduction of Ti and Si. *J. Phys. Chem. C* **2007**, *111*, 16477–16488. [CrossRef]
22. Seriani, N. Ab Initio Simulations of Water Splitting on Hematite. *J. Phys. Condens. Matter* **2017**, *29*, 463002. [CrossRef]
23. Li, X.; Yu, J.; Low, J.; Fang, Y.; Xiao, J.; Chen, X. Engineering Heterogeneous Semiconductors for Solar Water Splitting. *J. Mater. Chem. A* **2015**, *3*, 2485–2534. [CrossRef]
24. Phuan, Y.W.; Ong, W.-J.; Chong, M.N.; Ocon, J.D. Prospects of electrochemically synthesized hematite photoanodes for photoelectrochemical water splitting: A review. *J. Photochem. Photobiol. C Photochem. Rev.* **2017**, *33*, 54–82. [CrossRef]
25. Bryan, D.; Gamelin, D.R. Doped Semiconductor Nanocrystals: Synthesis, Characterization, Physical Properties, and Applications. *Prog. Inorg. Chem.* **2005**, *54*, 47–126.
26. Queisser, H.J.; Haller, E.E. Defects in Semiconductors: Some Fatal, Some Vital. *Science* **1998**, *281*, 945–950. [CrossRef] [PubMed]
27. Cheng, W.; He, J.; Sun, Z.; Peng, Y.; Yao, T.; Liu, Q.; Jiang, Y.; Hu, F.; Xie, Z.; He, B.; et al. Ni-Doped Overlayer Hematite Nanotube: A Highly Photoactive Architecture for Utilization of Visible Light. *J. Phys. Chem. C* **2012**, *116*, 24060–24067. [CrossRef]
28. Deng, J.; Zhong, J.; Pu, A.; Zhang, D.; Li, M.; Sun, X.; Lee, S.-T. Ti-Doped Hematite Nanostructures for Solar Water Splitting with High Efficiency. *J. Appl. Phys.* **2012**, *112*, 084312. [CrossRef]
29. Hu, Y.-S.; Kleiman-Shwarsctein, A.; Forman, A.J.; Hazen, D.; Park, J.-N.; McFarland, E.W. Pt-Doped α-Fe_2O_3 Thin Films Active for Photoelectrochemical Water Splitting. *Chem. Mater.* **2008**, *20*, 3803–3805. [CrossRef]
30. Wang, J.; Sun, H.; Huang, J.; Li, Q.; Yang, J. Band Structure Tuning of Tio2 for Enhanced Photoelectrochemical Water Splitting. *J. Phys. Chem. C* **2014**, *118*, 7451–7457. [CrossRef]
31. Nagaveni, K.; Hegde, M.; Madras, G. Structure and Photocatalytic Activity of $Ti_{1-X}M_XO_{2\pm\Delta}$ (M = W, V, Ce, Zr, Fe, and Cu) Synthesized by Solution Combustion Method. *J. Phys. Chem. B* **2004**, *108*, 20204–20212. [CrossRef]
32. Chang, S.-M.; Liu, W.-S. Surface Doping Is More Beneficial Than Bulk Doping to the Photocatalytic Activity of Vanadium-Doped Tio_2. *Appl. Catal. B Environ.* **2011**, *101*, 333–342. [CrossRef]
33. Simfukwe, J.; Mapasha, R.E.; Braun, A.; Diale, M. Density Functional Theory Study of Cu Doped {0001} and {01-1 2} Surfaces of Hematite for Water Splitting. *MRS Adv.* **2018**, *3*, 669–678. [CrossRef]
34. Kayes, B.M.; Atwater, H.A.; Lewis, N.S. Comparison of the Device Physics Principles of Planar and Radial P-N Junction Nanorod Solar Cells. *J. Appl. Phys.* **2005**, *97*, 114302. [CrossRef]
35. McDonald, K.J.; Choi, K.-S. Synthesis and Photoelectrochemical Properties of Fe2O3/ZnFe2O4Composite Photoanodes for Use in Solar Water Oxidation. *Chem. Mater.* **2011**, *23*, 4863–4869. [CrossRef]
36. Miao, C.; Ji, S.; Xu, G.; Liu, G.; Zhang, L.; Ye, C. Micro-Nano-Structured Fe2o3: Ti/Znfe2o4 Heterojunction Films for Water Oxidation . *ACS Appl. Mater. Interfaces* **2012**, *4*, 4428–4433. [CrossRef] [PubMed]
37. Pan, H.; Gu, B.; Eres, G.; Zhang, Z. Ab initio study on noncompensated CrO codoping of GaN for enhanced solar energy conversion. *J. Chem. Phys.* **2010**, *132*, 104501. [CrossRef]
38. Yin, W.-J.; Tang, H.; Wei, S.-H.; Al-Jassim, M.M.; Turner, J.; Yan, Y. Band Structure Engineering of Semiconductors for Enhanced Photoelectrochemical Water Splitting: The Case of TiO_2. *Phys. Rev. B* **2010**, *82*, 045106. [CrossRef]

39. Gai, Y.; Li, J.; Li, S.-S.; Xia, J.-B.; Wei, S.-H. Design of Narrow-Gap Tio 2: A Passivated Codoping Approach for Enhanced Photoelectrochemical Activity. *Phys. Rev. Lett.* **2009**, *102*, 036402. [CrossRef] [PubMed]
40. Kaouk, A.; Ruoko, T.-P.; Pyeon, M.; Gönüllü, Y.; Kaunisto, K.; Lemmetyinen, H.; Mathur, S. High Water-Splitting Efficiency through Intentional in and Sn Codoping in Hematite Photoanodes. *J. Phys. Chem. C* **2016**, *120*, 28345–28353. [CrossRef]
41. Wang, J.; Du, C.; Peng, Q.; Yang, J.; Wen, Y.; Shan, B.; Chen, R. Enhanced photoelectrochemical water splitting performance of hematite nanorods by Co and Sn co-doping. *Int. J. Hydrogen Energy* **2017**, *42*, 29140–29149. [CrossRef]
42. Zhang, M.; Luo, W.; Li, Z.; Yu, T.; Zou, Z. Improved Photoelectrochemical Responses of Si and Ti Codoped A-Fe_2O_3 Photoanode Films. *Appl. Phys. Lett.* **2010**, *97*, 042105. [CrossRef]
43. Zhu, W.; Qiu, X.; Iancu, V.; Chen, X.-Q.; Pan, H.; Wang, W.; Dimitrijevic, N.M.; Rajh, T.; Meyer, H.M., III; Paranthaman, M.P. Band Gap Narrowing of Titanium Oxide Semiconductors by Noncompensated Anion-Cation Codoping for Enhanced Visible-Light Photoactivity. *Phys. Rev. Lett.* **2009**, *103*, 226401. [CrossRef] [PubMed]
44. Choudhuri, I.; Patra, N.; Mahata, A.; Ahuja, R.; Pathak, B. B–N@Graphene: Highly Sensitive and Selective Gas Sensor. *J. Phys. Chem. C* **2015**, *119*, 24827–24836. [CrossRef]
45. Garg, P.; Kumar, S.; Choudhuri, I.; Mahata, A.; Pathak, B. Hexagonal Planar Cds Monolayer Sheet for Visible Light Photocatalysis. *J. Phys. Chem. C* **2016**, *120*, 7052–7060. [CrossRef]
46. Mahata, A.; Rai, R.K.; Choudhuri, I.; Singh, S.K.; Pathak, B.; Vs, D. Indirect Pathway for Nitrobenzene Reduction Reaction on a Ni Catalyst Surface: A Density Functional Study. *Phys. Chem. Chem. Phys.* **2014**, *16*, 26365–26374. [CrossRef]
47. Henkelman, G.; Arnaldsson, A.; Jónsson, H. A fast and robust algorithm for Bader decomposition of charge density. *Comput. Mater. Sci.* **2006**, *36*, 354–360. [CrossRef]
48. Qi, X.; She, G.; Wang, M.; Mu, L.; Shi, W. Electrochemical Synthesis of P-Type Zn-Doped A-Fe_2O_3 Nanotube Arrays for Photoelectrochemical Water Splitting. *Chem. Commun.* **2013**, *49*, 5742–5744. [CrossRef] [PubMed]
49. Ingler, W.B., Jr.; Khan, S.U. A Self-Driven P/N-Fe_2O_3 Tandem Photoelectrochemical Cell for Water Splitting, Electrochemical and Solid. *State Lett.* **2006**, *9*, G144. [CrossRef]
50. Kumar, P.; Sharma, P.; Shrivastav, R.; Dass, S.; Satsangi, V.R. Electrodeposited Zirconium-Doped A-Fe_2O_3 Thin Film for Photoelectrochemical Water Splitting. *Int. J. Hydrog. Energy* **2011**, *36*, 2777–2784. [CrossRef]
51. Shen, S.; Guo, P.; Wheeler, D.A.; Jiang, J.; Lindley, S.A.; Kronawitter, C.X.; Zhang, J.Z.; Guo, L.; Mao, S.S. Physical and Photoelectrochemical Properties of Zr-Doped Hematite Nanorod Arrays. *Nanoscale* **2013**, *5*, 9867–9874. [CrossRef]
52. Hohenberg, P.; Kohn, W. Density Functional Theory (Dft). *Phys. Rev.* **1964**, *136*, B864. [CrossRef]
53. Kohn, W.; Sham, L.J. Self-Consistent Equations Including Exchange and Correlation Effects. *Phys. Rev.* **1965**, *140*, A1133. [CrossRef]
54. Giannozzi, P.; Baroni, S.; Bonini, N.; Calandra, M.; Car, R.; Cavazzoni, C.; Ceresoli, D.; Chiarotti, G.L.; Cococcioni, M.; Dabo, I.; et al. QUANTUM ESPRESSO: A modular and open-source software project for quantum simulations of materials. *J. Phys. Condens. Matter* **2009**, *21*, 395502. [CrossRef]
55. Vanderbilt, D. Soft self-consistent pseudopotentials in a generalized eigenvalue formalism. *Phys. Rev. B* **1990**, *41*, 7892–7895. [CrossRef] [PubMed]
56. Perdew, J.P.; Burke, K.; Ernzerhof, M. Generalized Gradient Approximation Made Simple. *Phys. Rev. Lett.* **1996**, *77*, 3865–3868. [CrossRef]
57. Anisimov, V.I.; Solovyev, I.; Korotin, M.; Czyżyk, M.; Sawatzky, G. Density-Functional Theory and Nio Photoemission Spectra. *Phys. Rev. B* **1993**, *48*, 16929. [CrossRef]
58. Anisimov, V.I.; Zaanen, J.; Andersen, O.K. Band Theory and Mott Insulators: Hubbard U Instead of Stoner I. *Phys. Rev. B* **1991**, *44*, 943. [CrossRef]
59. Himmetoglu, B.; Floris, A.; de Gironcoli, S.; Cococcioni, M. Hubbard-Corrected Dft Energy Functionals: The Lda+ U Description of Correlated Systems. *Int. J. Quantum Chem.* **2014**, *114*, 14–49. [CrossRef]
60. Antonov, V.; Harmon, B.; Yaresko, A. *Electronic Structure and Magneto-Optical Properties of Solids*; Springer: Berlin, Germany, 2004.
61. Hubbard, J. Electron correlations in narrow energy bands. *Proc. R. Soc. London. Ser. A Math. Phys. Sci.* **1963**, *276*, 238–257. [CrossRef]
62. Hubbard, J. The approximate calculation of electronic band structure. *Proc. Phys. Soc.* **1967**, *92*, 921–937. [CrossRef]
63. Dzade, N.Y.; Roldan, A.; De Leeuw, N.H. A Density Functional Theory Study of the Adsorption of Benzene on Hematite (α-Fe2O3) Surfaces. *Minerals* **2014**, *4*, 89–115. [CrossRef]
64. Rohrbach, A.; Hafner, J.; Kresse, G. Ab Initio Study of the (0001) Surfaces of Hematite and Chromia: Influence of Strong Electronic Correlations. *Phys. Rev. B* **2004**, *70*, 125426. [CrossRef]
65. Bandyopadhyay, A.; Velev, J.; Butler, W.; Sarker, S.K.; Bengone, O. Effect of Electron Correlations on the Electronic and Magnetic Structure of Ti-Doped A-Hematite. *Phys. Rev. B* **2004**, *69*, 174429. [CrossRef]
66. Monkhorst, H.J.; Pack, J.D. Special points for Brillouin-zone integrations. *Phys. Rev. B* **1976**, *13*, 5188–5192. [CrossRef]